General Field Theory Treatment of *E*-Plane Waveguide Junction Circulators—Part I: Full-Height Ferrite Configuration

M. EZZAT EL-SHANDWILY, MEMBER, IEEE, AHMAD A. KAMAL, MEMBER, IEEE, AND ESMAT A. F. ABDALLAH, STUDENT MEMBER, IEEE

Abstract—**In this paper an exact field theory treatment for the *N*-port *E*-plane full-height ferrite rod junction circulators is presented. Field expressions are written in each region of the junction in the form of infinite modes. Matching of the fields at the common boundaries is used to get a set of infinite nonhomogeneous equations in these mode amplitudes.**

The point matching technique is used to obtain an approximate solution for the field amplitudes by taking a finite number of modes in each region. Three types of junctions have been analyzed by this technique. These junctions are the symmetrical Y junction and two types of T junctions. Experimental measurements have been carried out to verify the obtained numerical results.

I. Introduction

THE *H*-PLANE waveguide junction circulator, which has been extensively studied by many investigators, is not capable of handling large powers. To meet the requirements of high-power radar systems, *E*-plane junction circulators have to be used.

A number of authors have made brief investigations of the *E*-plane junction circulators [1]–[8], such references are of an experimental nature. A theoretical treatment of this structure appears to be exceedingly complex since the RF field varies along the direction of the applied static magnetic field. As a result most waveguide single-junction circulators are of the *H*-plane type, and, therefore, much more design information and practical knowledge are available for this type. However, as the high-peak-power requirements increase, the problem of RF high-voltage breakdown becomes a critical factor, since the location of the ferrite material in the *H*-plane configuration is at the point of maximum electric field intensity. In the *E*-plane configuration the ferrite is not located near this point of maximum intensity, which decreases the tendency for RF high-power breakdown. In addition, RF losses caused by the dielectric properties of both the ferrite and any dielectric loading materials will be smaller, thereby reducing the heating effects.

It is the aim of this paper to present, for the first time, a field theory treatment of full-height *E*-plane waveguide junction circulators. It is the authors' belief that this novel work will have an important impact on the design of these types of circulators.

Manuscript received January 29, 1976; revised October 12, 1976.

M. E. El-Shandwily was with the Electrical and Electronic Research Laboratory, National Research Center, Cairo, Egypt. He is now with the Electrical Engineering Department, University of Technology, Tal Mohammad, Baghdad, Iraq.

A. A. Kamal is with the Department of Electronic Engineering, Cairo University, Cairo, Egypt.

E. A. F. Abdallah is with the Electrical and Electronic Research Laboratory, National Research Center, Cairo, Egypt.

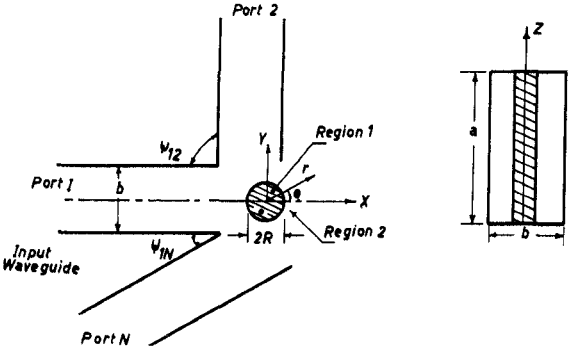

Fig. 1. Schematic representation of an *E*-plane nonsymmetrical waveguide junction circulator.

The circulator consists of N waveguides intersecting as shown schematically in Fig. 1. The ferrite rod is placed inside the junction and the dc magnetic field is applied normal to the plane of the junction. In general, the waveguides need not be symmetrically located around the junction. The system is assumed to be free of any losses and excitation by the dominant TE_{10} mode as only one of the waveguides takes place. It is further assumed that the output ports are perfectly matched and the electromagnetic field components have a time dependence in the form of exp ($j\omega t$). Since the electromagnetic fields are variable along the normal to the junction (the z axis) all the TE_{1q} and TM_{1p} waveguide modes will be excited such that the boundary conditions are always satisfied.

Matching of the fields takes place at the ferrite–air interface and at the common boundaries between the junction and the waveguides. Thus it is possible to obtain the magnitudes and phases of the electromagnetic field components at each point within the junction. By this technique, one can obtain the circulator characteristics (reflection coefficient, isolation, and insertion loss) for different operating conditions (ferrite radius, applied dc magnetic field, and physical properties of ferrite materials used).

This technique has been applied successfully by the authors for the analysis of the *H*-plane waveguide junction circulators [9].

II. Theoretical Analysis of *N*-Port Circulators

To write complete expressions for the electromagnetic field components in the ferrite rod (region 1, see Fig. 1), it is

assumed that the field components have exp $(-j\beta z)$ dependence for waves propagating upwards. Since there is a perfect conductor at the upper and lower ends of the ferrite rod, there will be another wave reflected downwards and the field components have exp $(j\beta z)$ dependence.

The coupled wave equations in the ferrite rod can be written as [10]

$$\nabla^2_{r,\theta} E_z^f + aE_z^f + bH_z^f = 0 \tag{1a}$$

$$\nabla^2_{r,\theta} H_z^f + cH_z^f + dE_z^f = 0 \tag{1b}$$

where

$$a = -\beta^2 + \omega^2 \varepsilon_0 \varepsilon_f \mu_0 \left(\frac{\mu^2 - K^2}{\mu}\right)$$

$$b = j\beta\omega\mu_0 K/\mu$$

$$c = \frac{1}{\mu}(-\beta^2 + \omega^2 \mu_0 \mu \varepsilon_0 \varepsilon_f)$$

$$d = -j\beta\omega\varepsilon_0 \varepsilon_f K/\mu$$

and

μ, K diagonal and off-diagonal permeability tensor components, respectively,

ε_f relative permittivity of ferrite material.

When solving (1a,b) using Kale's theorem [10] one gets

$$E_z^f|_I = [A_{n1} J_n(K_{c1} r) + A_{n2} J_n(K_{c2} r)] \cdot \exp[j(n\theta - \beta z)] \tag{2a}$$

$$H_z^f|_I = [D_1 A_{n1} J_n(K_{c1} r) + D_2 A_{n2} J_n(K_{c2} r)] \cdot \exp[j(n\theta - \beta z)] \tag{2b}$$

where the subscript I denotes a wave propagating in the positive Z direction and the superscript f denotes the ferrite material, and

$$D_{1,2} = \frac{\mu}{j\beta\mu_0\omega K}[K^2_{c1,2} + \beta^2 - \omega^2\varepsilon_0\varepsilon_f\mu_0(\mu^2 - K^2)/\mu] \tag{3}$$

$$K^2_{c1,2} = \frac{1}{2}\left[-\beta^2\left(1 + \frac{1}{\mu}\right) + \omega^2\varepsilon_0\mu_0\varepsilon_f(\mu^2 - K^2)/\mu + \omega^2\mu_0\varepsilon_0\varepsilon_f\right] \pm \left\{\left[-\beta^2\left(1 - \frac{1}{\mu}\right) + \omega^2\varepsilon_0\mu_0\varepsilon_f(\mu^2 - K^2)/\mu - \omega^2\mu_0\varepsilon_0\varepsilon_f\right]^2 + \beta^2\omega^2\varepsilon_0\varepsilon_f\mu_0(K/\mu)^2\right\}^{1/2} \tag{4}$$

where

A_{n1}, A_{n2} complex amplitudes,

$J_n(K_{c1,2} r)$ Bessel's function of the first kind and order n with n real integers.

Since the longitudinal components $E_z^f|_I$ and $H_z^f|_I$ are now known the transverse components are found from Maxwell's equations.

The perfect conductor, at $z = 0$ and $z = a$, represents a short circuit to the propagating waves, therefore, there is another wave, wave II, propagating downwards in the $-Z$ direction and which has exp $(j\beta z)$ dependence. The longitudinal field components for this wave may be obtained from (2a,b) by using $-\beta$ instead of β.

The tangential electric field components should have a value of zero on the common perfect conducting walls of the junction. To satisfy these boundary conditions, the propagation constant β in the ferrite rod in the Z direction should have the following values:

$$\beta = \frac{m\pi}{a}, \qquad m = 0, 1, 2, \cdots, \infty \tag{5}$$

which depends only on the dimension a of the waveguide.

The resulting field distribution in the ferrite rod takes the following form:

$$E_z^f(r,\theta,z) = 2\sum_{m=0}^{\infty}\sum_{n=-\infty}^{\infty}[A_{m,n1} J_n(K_{c1} r) + A_{m,n2} J_n(K_{c2} r)]e^{jn\theta}\cos\frac{m\pi z}{a} \tag{6}$$

$$H_z^f(r,\theta,z) = -2j\sum_{m=0}^{\infty}\sum_{n=-\infty}^{\infty}[D_1 A_{m,n1} J_n(K_{c1} r) + D_2 A_{m,n2} J_n(K_{c2} r)]e^{jn\theta}\sin\frac{m\pi z}{a} \tag{7}$$

$$E_\theta^f(r,\theta,z) = 2j\sum_{m=0}^{\infty}\sum_{n=-\infty}^{\infty}\left\{A_{m,n1}\left[\bar{Q}K_{c1}J_n'(K_{c1}r) - \frac{jnG}{r}J_n(K_{c1}r) + SD_1K_{c1}J_n'(K_{c1}r) - \frac{jn\bar{R}}{r}D_1J_n(K_{c1}r)\right] + A_{m,n2}\left[\bar{Q}K_{c2}J_n'(K_{c2}r) - \frac{jnG}{r}J_n(K_{c2}r) + SD_2K_{c2}J_n'(K_{c2}r) - \frac{jn\bar{R}}{r}D_2J_n(K_{c2}r)\right]\right\}e^{jn\theta}\sin\frac{m\pi z}{a} \tag{8}$$

$$H_\theta^f(r,\theta,z) = 2\sum_{m=0}^{\infty}\sum_{n=-\infty}^{\infty}\left\{A_{m,n1}\left[-UK_{c1}J_n'(K_{c1}r) + \frac{jnT}{r}J_n(K_{c1}r) - \bar{Q}D_1K_{c1}J_n'(K_{c1}r) + \frac{jnG}{r}D_1J_n(K_{c1}r)\right] + A_{m,n2}\left[-UK_{c2}J_n'(K_{c2}r) + \frac{jnT}{r}J_n(K_{c2}r) - \bar{Q}D_2K_{c2}J_n'(K_{c2}r) + \frac{jnG}{r}D_2J_n(K_{c2}r)\right]\right\}e^{jn\theta}\cos\frac{m\pi z}{a} \tag{9}$$

where

$$G = -j\beta(-\beta^2 + \omega^2\mu_0\mu\varepsilon_0\varepsilon_f)\Delta^{-1}$$
$$\bar{Q} = \beta\omega^2\varepsilon_0\varepsilon_f\mu_0 K\Delta^{-1}$$
$$\bar{R} = -\omega\mu_0 K\beta^2\Delta^{-1}$$
$$S = -j\omega[-\mu_0\mu\beta^2 + \omega^2\mu_0^2(\mu^2 - K^2)\varepsilon_0\varepsilon_f]\Delta^{-1}$$
$$T = \omega^3\varepsilon_0^2\varepsilon_f^2\mu_0 K\Delta^{-1}$$
$$U = j\omega[-\varepsilon_0\varepsilon_f\beta^2 + \omega^2\varepsilon_0^2\varepsilon_f^2\mu_0\mu]\Delta^{-1}$$
$$\Delta = [-\beta^2 + \omega^2\varepsilon_0\varepsilon_f\mu_0(\mu + K)] \cdot [-\beta^2 + \omega^2\varepsilon_0\varepsilon_f\mu_0(\mu - K)].$$

When a similar procedure is followed in the air region (region 2), one obtains the following electromagnetic field distributions:

$$E_z^a(r,\theta,z) = 2\sum_{m=0}^{\infty}\sum_{n=-\infty}^{\infty}[F_{m,n1}J_n(K_a r) + F_{m,n2}Y_n(K_a r)]e^{jn\theta}\cos\frac{m\pi z}{a} \tag{10}$$

$$H_z^a(r,\theta,z) = -2j\sum_{m=0}^{\infty}\sum_{n=-\infty}^{\infty}[H_{m,n1}J_n(K_a r) + H_{m,n2}Y_n(K_a r)]e^{jn\theta}\sin\frac{m\pi z}{a} \tag{11}$$

$$E_\theta^a(r,\theta,z) = -2j\sum_{m=0}^{\infty}\sum_{n=-\infty}^{\infty}\left\{F_{m,n1}\frac{jnG_a}{r}J_n(K_a r) + F_{m,n2}\frac{jnG_a}{r}Y_n(K_a r) - H_{m,n1}S_a K_a J_n'(K_a r) - H_{m,n2}S_a K_a Y_n'(K_a r)\right\}e^{jn\theta}\sin\frac{m\pi z}{a} \tag{12}$$

$$H_\theta^a(r,\theta,z) = 2\sum_{m=0}^{\infty}\sum_{n=-\infty}^{\infty}\left\{-F_{m,n1}U_a K_a J_n'(K_a r) - F_{m,n2}U_a K_a Y_n'(K_a r) + H_{m,n1}\frac{jnG_a}{r}J_n(K_a r) + H_{m,n2}\frac{jnG_a}{r}Y_n(K_a r)\right\}e^{jn\theta}\cos\frac{m\pi z}{a} \tag{13}$$

where

$$K_a^2 = \omega^2\varepsilon_0\mu_0 - \beta_a^2$$
$$\beta_a = \frac{m\pi}{a}$$
$$G_a = -j\beta_a/K_a^2$$
$$S_a = -j\omega\mu_0/K_a^2$$
$$U_a = j\omega\varepsilon_0/K_a^2$$

and

$F_{m,n1}, F_{m,n2}, H_{m,n1}, H_{m,n2}$ complex constants to be determined.

The other two components, namely E_r^a and H_r^a, are not written because they are not needed.

Up to now, all the expressions for the field distributions inside the ferrite rod (region 1) and the air ring surrounding the ferrite rod (region 2) have been written. The complex amplitudes $F_{m,n1}$, $F_{m,n2}$, $H_{m,n1}$, and $H_{m,n2}$ can be obtained in terms of $A_{m,n1}$ and $A_{m,n2}$ from the continuity conditions of the tangential electromagnetic field components at the ferrite–air interface. The resulting expressions are very long and for the sake of brevity they will not be written here.

Assume the junction to be excited by the dominant TE_{10} mode from waveguide 1, Fig. 1, which is the only propagating mode assumed. The incident electromagnetic field components are given by

$$H_z^i(x_1,z) = K_{10}\sin\frac{\pi z}{a}\exp(-jK_d x_1) \tag{14}$$

$$E_y^i(x_1,z) = \frac{\omega\mu_0}{K_d}K_{10}\sin\frac{\pi z}{a}\exp(-jK_d x_1) \tag{15}$$

$$H_x^i(x_1,z) = \frac{-jK_{10}^2}{K_d}\cos\frac{\pi z}{a}\exp(-jK_d x_1) \tag{16}$$

where

$$K_{10} = \pi/a$$
$$K_d = \sqrt{\omega^2\mu_0\varepsilon_0 - K_{10}^2}.$$

The junction and the ferrite post represent a discontinuity to the incident field on port 1, and therefore scattered fields are introduced in all waveguides. Since the incident electromagnetic field components vary along the Z direction, the scattered fields are represented by both transverse electric and transverse magnetic waveguide modes. The scattered field in waveguide 1 represents the reflected wave, while the scattered field in any other waveguide represents the transmission to this waveguide. The scattered field in waveguide 1 can be written as follows.

For TM_{pq} *Modes:*

$$E_z(x_1,y_1,z) = -\sum_{p=1}^{\infty}\sum_{q=1}^{\infty}a_{pq}\frac{p\pi}{a}\cos\frac{p\pi z}{a} \cdot \sin\left[\frac{q\pi}{b}\left(y_1 + \frac{b}{2}\right)\right]e^{\Gamma_{pq}x_1} \tag{17}$$

$$E_y(x_1,y_1,z) = -\sum_{p=1}^{\infty}\sum_{q=1}^{\infty}a_{pq}\frac{q\pi}{b}\sin\frac{p\pi z}{a} \cdot \cos\left[\frac{q\pi}{b}\left(y_1 + \frac{b}{2}\right)\right]e^{\Gamma_{pq}x_1} \tag{18}$$

$$H_z(x_1,y_1,z) = \sum_{p=1}^{\infty}\sum_{q=1}^{\infty}a_{pq}\frac{j\omega\varepsilon_0}{\Gamma_{pq}}\frac{q\pi}{b}\sin\frac{p\pi z}{a} \cdot \cos\left[\frac{q\pi}{b}\left(y_1 + \frac{b}{2}\right)\right]e^{\Gamma_{pq}x_1} \tag{19}$$

$$H_y(x_1,y_1,z) = -\sum_{p=1}^{\infty}\sum_{q=1}^{\infty}a_{pq}\frac{j\omega\varepsilon_0}{\Gamma_{pq}}\frac{p\pi}{a}\cos\frac{p\pi z}{a} \cdot \sin\left[\frac{q\pi}{b}\left(y_1 + \frac{b}{2}\right)\right]e^{\Gamma_{pq}x_1} \tag{20}$$

$$E_x(x_1,y_1,z) = -\sum_{p=1}^{\infty}\sum_{q=1}^{\infty} a_{pq}\frac{K_{pq}^2}{\Gamma_{pq}}\sin\frac{p\pi z}{a} \cdot \sin\left[\frac{q\pi}{b}\left(y_1+\frac{b}{2}\right)\right]e^{\Gamma_{pq}x_1} \tag{21}$$

$$H_x(x_1,y_1,z) = 0. \tag{22}$$

For TE_{pq} *Modes:*

$$H_z(x_1,y_1,z) = \sum_{p=0}^{\infty}\sum_{q=0}^{\infty} b_{pq}\frac{p\pi}{a}\sin\frac{p\pi z}{a} \cdot \cos\left[\frac{q\pi}{b}\left(y_1+\frac{b}{2}\right)\right]e^{\Gamma_{pq}x_1} \tag{23}$$

$$H_y(x_1,y_1,z) = \sum_{p=0}^{\infty}\sum_{q=0}^{\infty} b_{pq}\frac{q\pi}{b}\cos\frac{p\pi z}{a} \cdot \sin\left[\frac{q\pi}{b}\left(y_1+\frac{b}{2}\right)\right]e^{\Gamma_{pq}x_1} \tag{24}$$

$$E_z(x_1,y_1,z) = \sum_{p=0}^{\infty}\sum_{q=0}^{\infty} b_{pq}\frac{j\omega\mu_0}{\Gamma_{pq}}\frac{q\pi}{b}\cos\frac{p\pi z}{a} \cdot \sin\left[\frac{q\pi}{b}\left(y_1+\frac{b}{2}\right)\right]e^{\Gamma_{pq}x_1} \tag{25}$$

$$E_y(x_1,y_1,z) = -\sum_{p=0}^{\infty}\sum_{q=0}^{\infty} b_{pq}\frac{j\omega\mu_0}{\Gamma_{pq}}\frac{p\pi}{a}\sin\frac{p\pi z}{a} \cdot \cos\left[\frac{q\pi}{b}\left(y_1+\frac{b}{2}\right)\right]e^{\Gamma_{pq}x_1} \tag{26}$$

$$H_x(x_1,y_1,z) = -\sum_{p=0}^{\infty}\sum_{q=0}^{\infty} b_{pq}\frac{K_{pq}^2}{\Gamma_{pq}}\cos\frac{p\pi z}{a} \cdot \cos\left[\frac{q\pi}{b}\left(y_1+\frac{b}{2}\right)\right]e^{\Gamma_{pq}x_1} \tag{27}$$

$$E_x(x_1,y_1,z) = 0 \tag{28}$$

where

$$\Gamma_{pq}^2 = K_{pq}^2 - \omega^2\varepsilon_0\mu_0$$

$$K_{pq}^2 = \left(\frac{p\pi}{a}\right)^2 + \left(\frac{q\pi}{b}\right)^2$$

and

b_{10} complex reflection coefficient at the input port,
a_{pq}, b_{pq} complex amplitudes of the evanescent modes for the transverse magnetic and transverse electric modes, respectively.

For the other waveguides, the same expressions are used for the electromagnetic field components, except that (x_2,y_2,z), (x_3,y_3,z), $\cdots$, (x_N,y_N,z) is written instead of (x_1,y_1,z). These new axes result from rotating the previous axes (x_1,y_1,z) by angles $\psi_{12}, \psi_{13}, \cdots, \psi_{1N}$, which are the angles between the input waveguide and the other waveguides.

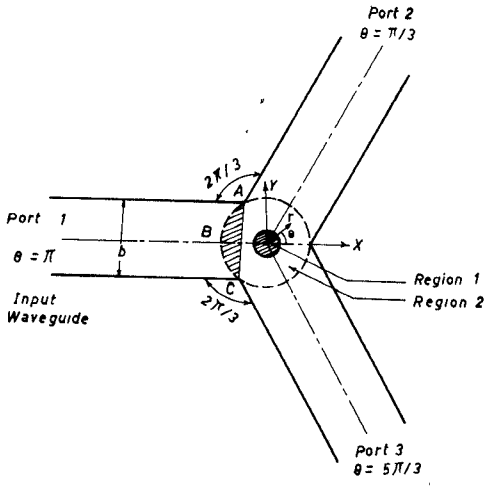

Fig. 2. Schematic representation of an *E*-plane Y-junction circulator.

Up to this point the analysis is general and it neither depends on the number of ports nor the junction symmetry. In order to match the fields in the air surrounding the ferrite rod and the waveguide fields, a boundary between both regions should be chosen. This imaginary boundary depends on the geometry of the junction. Thus each of the junctions should be treated separately. The Y junction is chosen as an example of the symmetrical junctions, while the T junction is chosen as an example of the nonsymmetrical junctions.

A. The Full-Height Y*-Junction Circulator*

The waveguide equations hold up to the line AC, Fig. 2, while the field distribution in region 2 holds up to the arc ABC. They have a common area, in the shape of a segment of a circle (the same is true for ports 2 and 3), bounded by AC and ABC in which both representations are valid and complete. Any arbitrary boundary in this region, shown shaded in Fig. 2, may be chosen for convenience for field matching. It may be the surface AC, the surface $r = b/\sqrt{3}$, or any other surface in between. But outside the segment only one or the other representation is valid, so the matching must be done in the prescribed segment [11].

In this problem, the imaginary wall between region 2 and the waveguides is chosen to be a cylindrical wall [9]. The axis of this cylindrical surface coincides with the junction axis and its radius is $b/\sqrt{3}$ as shown by the dotted line in Fig. 2. Between each waveguide and region 2 there are four boundary conditions; namely:

$$E_z(r,\theta,z)\big|_{\text{region 2}} = E_z(x_i,y_i,z)\big|_{\text{waveguide } i} \tag{29}$$

$$H_z(r,\theta,z)\big|_{\text{region 2}} = H_z(x_i,y_i,z)\big|_{\text{waveguide } i} \tag{30}$$

$$E_\theta(r,\theta,z)\big|_{\text{region 2}} = E_y(x_i,y_i,z)\cos\theta_i - E_x(x_i,y_i,z)\sin\theta_i\big|_{\text{waveguide } i} \tag{31}$$

$$H_\theta(r,\theta,z)\big|_{\text{region 2}} = H_y(x_i,y_i,z)\cos\theta_i - H_x(x_i,y_i,z)\sin\theta_i\big|_{\text{waveguide } i} \tag{32}$$

where

$$i = 1,2,3$$
$$r = b/\sqrt{3}$$
$$x_i = b\cos\theta_i/\sqrt{3}$$
$$y_i = b\sin\theta_i/\sqrt{3}$$
$$\theta_i = \theta - (i-1)\frac{2\pi}{3}, \qquad \frac{2\pi}{3} \le \theta_i \le \frac{4\pi}{3}.$$

For the input waveguide (waveguide 1), substitute (10)–(13) and (17)–(28) into the four boundary conditions (29)–(32). Then using the orthogonality properties of the exponential and trigonometric functions the following equations are obtained:

$$2\sum_{n=-\infty}^{\infty}\left[F_{m,n1}J_n\left(K_a\frac{b}{\sqrt{3}}\right)+F_{m,n2}Y_n\left(K_a\frac{b}{\sqrt{3}}\right)\right]\exp(jn\theta)$$
$$+\sum_{q=0}^{\infty}\left\{-\frac{j\omega\mu_0}{\Gamma_{mq}}b_{mq}\frac{q\pi}{b}\sin\left[q\pi\left(\frac{\sin\theta}{\sqrt{3}}+\frac{1}{2}\right)\right]\right.$$
$$\left.+a_{mq}\frac{m\pi}{a}\sin\left[q\pi\left(\frac{\sin\theta}{\sqrt{3}}+\frac{1}{2}\right)\right]\right\}$$
$$\cdot\exp(\Gamma_{mq}b\cos\theta/\sqrt{3})=0 \quad (33)$$

$$2j\sum_{n=-\infty}^{\infty}\left[H_{m.n1}J_n\left(K_a\frac{b}{\sqrt{3}}\right)+H_{m,n2}Y_n\left(K_a\frac{b}{\sqrt{3}}\right)\right]\exp(jn\theta)$$
$$+\sum_{q=0}^{\infty}\left\{\frac{j\omega\varepsilon_0}{\Gamma_{mq}}a_{mq}\frac{q\pi}{b}\cos\left[q\pi\left(\frac{\sin\theta}{\sqrt{3}}+\frac{1}{2}\right)\right]\right.$$
$$\left.+\frac{m\pi}{a}b_{mq}\cos\left[q\pi\left(\frac{\sin\theta}{\sqrt{3}}+\frac{1}{2}\right)\right]\right\}$$
$$\cdot\exp(\Gamma_{mq}b\cos\theta/\sqrt{3})$$
$$=\delta_{1m}\left[-\frac{\pi}{a}\exp(-jK_db\cos\theta/\sqrt{3})\right] \quad (34)$$

$$-2j\sum_{n=-\infty}^{\infty}\left\{F_{m,n1}\left[\frac{jnG_a}{b/\sqrt{3}}J_n\left(K_a\frac{b}{\sqrt{3}}\right)\right]\right.$$
$$+F_{m,n2}\left[\frac{jnG_a}{b/\sqrt{3}}Y_n\left(K_a\frac{b}{\sqrt{3}}\right)\right]$$
$$-H_{m,n1}\left[S_aK_aJ_n'\left(K_a\frac{b}{\sqrt{3}}\right)\right]$$
$$\left.-H_{m,n2}\left[S_aK_aY_n'\left(K_a\frac{b}{\sqrt{3}}\right)\right]\right\}\exp(jn\theta)$$
$$+\sum_{q=0}^{\infty}\left\{a_{mq}\frac{q\pi}{b}\cos\left[q\pi\left(\frac{\sin\theta}{\sqrt{3}}+\frac{1}{2}\right)\right]\cos\theta\right.$$
$$-\frac{a_mq}{\Gamma_{mq}}K_{mq}^2\sin\left[q\pi\left(\frac{\sin\theta}{\sqrt{3}}+\frac{1}{2}\right)\right]\sin\theta$$
$$\left.+\frac{j\omega\mu_0}{\Gamma_{mq}}b_{mq}\frac{m\pi}{a}\cos\left[q\pi\left(\frac{\sin\theta}{\sqrt{3}}+\frac{1}{2}\right)\right]\cos\theta\right\}$$
$$\cdot\exp(\Gamma_{mq}b\cos\theta/\sqrt{3})$$
$$=\delta_{1m}\left[\frac{\omega\mu_0}{K_d}\frac{\pi}{a}\cos\theta\exp(-jK_db\cos\theta/\sqrt{3})\right] \quad (35)$$

$$2\sum_{n=-\infty}^{\infty}\left\{-F_{m,n1}\left[U_aK_aJ_n'\left(K_a\frac{b}{\sqrt{3}}\right)\right]\right.$$
$$-F_{m,n2}\left[U_aK_aY_n'\left(K_a\frac{b}{\sqrt{3}}\right)\right]$$
$$+H_{m,n1}\left[\frac{jnG_a}{b/\sqrt{3}}J_n\left(K_a\frac{b}{\sqrt{3}}\right)\right]$$
$$\left.+H_{m,n2}\left[\frac{jnG_a}{b/\sqrt{3}}Y_n\left(K_a\frac{b}{\sqrt{3}}\right)\right]\right\}\exp(jn\theta)$$
$$-\sum_{q=0}^{\infty}\left\{-j\omega\varepsilon_0\frac{a_mq}{\Gamma_{mq}}\frac{m\pi}{a}\right.$$
$$\cdot\sin\left[q\pi\left(\frac{\sin\theta}{\sqrt{3}}+\frac{1}{2}\right)\right]\cos\theta$$
$$+\frac{q\pi}{b}b_{mq}\sin\left[q\pi\left(\frac{\sin\theta}{\sqrt{3}}+\frac{1}{2}\right)\right]\cos\theta$$
$$\left.+b_{mq}K_{mq}^2\frac{1}{\Gamma_{mq}}\cos\left[q\pi\left(\frac{\sin\theta}{\sqrt{3}}+\frac{1}{2}\right)\right]\sin\theta\right\}$$
$$\cdot\exp(\Gamma_{mq}b\cos\theta/\sqrt{3})$$
$$=\delta_{1m}\left[\frac{jK_{10}^2}{K_d}\sin\theta\exp(-jK_db\cos\theta/\sqrt{3})\right] \quad (36)$$

where δ_{1m} is the Kronecker delta, which is equal to unity when $m = 1$ and zero for any other value of m. The right-hand-side term exists only for the input waveguide since it represents the incident TE_{10} wave on port 1.

For waveguide 2, in the boundary conditions substitute (29)–(32) when $i = 2$ with (10)–(13) and (17)–(28) to get equations (33)–(36); a_{mq} is replaced by a'_{mq}; b_{mq}, by b'_{mq}; and θ, by $(\theta + 2\pi/3)$. Similar equations are derived for waveguide 3, by replacing a_{mq} by a''_{mq}; b_{mq}, by b''_{mq}; and θ, by $(\theta + 4\pi/3)$. The right-hand side is always zero in these equations since there are no incident waves on ports 2 and 3.

One now has 12 infinite equations in the infinite number of unknowns a_{mq}, b_{mq}, a'_{mq}, b'_{mq}, a''_{mq}, b''_{mq}, $A_{m.n.1}$, and $A_{m,n2}$ ($F_{m,n1}, F_{m,n2}, H_{m,n1}$, and $H_{m.n2}$ have been obtained in terms of $A_{m,n1}$ and $A_{m,n2}$). For any value of m other than one, these equations represent a system of homogeneous equations. Since the determinant of their coefficient is not equal to zero, then there is only the trivial solution; i.e., all the complex amplitudes a_{mq}, b_{mq}, a'_{mq}, b'_{mq}, a''_{mq}, b''_{mq}, $A_{m.n1}$, and $A_{m.n2}$ are equal to zero. For $m = 1$, the above equations constitute a system of nonhomogeneous equations in these infinite unknowns and should have a unique solution. This result is expected since the incident TE_{10} mode excites only modes having the same type of variation with the Z direction due to the uniformity of the structure in this direction.

In order to have numerical results, use the point matching technique. Truncation in the eight infinite summations appearing in the above 12 equations should be done. Consider N cylindrical modes, Q transverse electric waveguide modes, and L transverse magnetic waveguide modes. For p matching points in each waveguide, the number of

equations is $12p$. For the number of equations to be equal to the number of unknowns, the following equation should be fulfilled:

$$12p = 2(2N + 1) + 3(Q + 1) + 3L. \tag{37}$$

It should be noted that for any value of p there are $2p$ possible solutions for (37).

B. The Full-Height T-*Junction Circulator*

Two types of T junctions have been studied. In the first type, shown in Fig. 3, the metallic boundary 1–4 is a plane surface. In the second type, Fig. 4, the metallic boundary 1–4 is a segment of a cylindrical wall. The imaginary boundary chosen for matching in both cases is a cylindrical surface of radius $b/\sqrt{2}$ [9]. Another condition that should be satisfied in both types of T junctions is that the tangential electric field $E_z(r,\theta,z)$ and $E_\theta(r,\theta,z)$ on the conducting surface 1–4 should be equal to zero. The boundary conditions for both types of T junctions are written as in (29)–(32) except that

$$r = b/\sqrt{2}$$
$$x_i = b \cos \theta_i/\sqrt{2}$$
$$y_i = b \sin \theta_i/\sqrt{2}$$
$$\theta_1 = \theta, \qquad 3\pi/4 \le \theta \le 5\pi/4$$
$$\theta_2 = \theta + \pi/2, \qquad \pi/4 \le \theta \le 3\pi/4$$
$$\theta_3 = \theta + 3\pi/2, \qquad 5\pi/4 \le \theta \le 7\pi/4.$$

For region 2 (boundary 1–4, Figs. 3 and 4),

$$E_z(r,\theta,z) = 0 \tag{38}$$
$$E_\theta(r,\theta,z) = 0 \tag{39}$$

where, for the first type of T junction,

$$r = b/2 \cos \theta, \qquad 7\pi/4 \le \theta \le \pi/4$$

and, for the second type of T junction,

$$r = b/\sqrt{2}, \qquad 7\pi/4 \le \theta \le \pi/4.$$

Applying the same technique as in the case of the Y-junction circulator, one gets a system of 14 nonhomogeneous equations. The number of unknowns is still the same as in the case of the Y junction. Assume p matching points in each waveguide and q matching points on the boundary 1–4, the number of equations is $(12p + 2q)$. In order to have a solution, the number of equations should be equal to the number of unknowns:

$$12p + 2q = 2(2N + 1) + 3(Q + 1) + 3L.$$

It should be noted that if the number of equations resulting from the matching points on the perfect conductor is taken to be equal to the number of cylindrical complex amplitudes, i.e., $2q = 2(2N + 1)$, then a set of $2q$ homogeneous equations results. The only solution for this set of equations is the trivial one, namely, $A_{m,n1} = A_{m,n2} = 0$. The transmission to the output ports, ports 2 and 3, is zero and complete reflection takes place from the input port. This of course is a wrong result, which is due to the incorrect choice of the number of matching points on each boundary and the number of unknowns to be determined. Similar conclusions have been reported by several investigators [12]–[14].

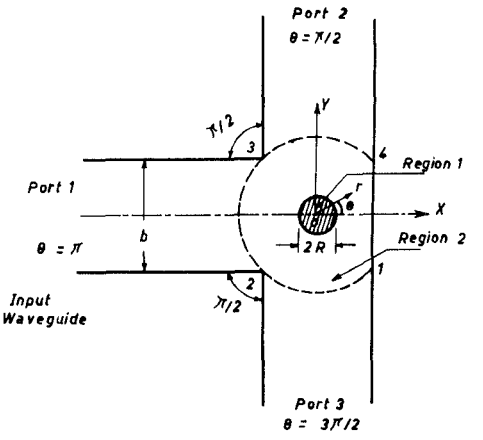

Fig. 3. Schematic representation of an *E*-plane T-junction circulator (first type).

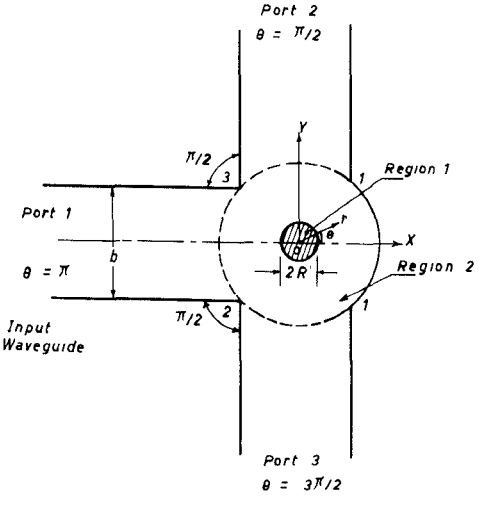

Fig. 4. Schematic representation of an *E*-plane T-junction circulator (second type).

III. Results and Discussions

In Section II, a system of infinite equations, with eight infinite unknowns, is obtained by applying the boundary conditions at all discontinuity surfaces as well as a chosen imaginary boundary whose shape is determined by the geometry of the junction. With a finite number of matching points chosen for each type of junction on the imaginary surface and truncation of the infinite summation, a system of nonhomogeneous linear equations is found. The simultaneous solution of these equations, using a digital computer, yields the circulator characteristics, namely, the reflection coefficient, isolation, and insertion loss.

The numerical calculations and experimental measurements have been carried out for the X-band frequency range and for two commercially available materials, the properties of which are given in Table I. The internal dc magnetic field used is 200 Oe. When this value was changed to 600 Oe the

TABLE I

Material	$4\pi M_s$ Gauss	ΔH Oersted	ε_r	tan δ
Y13A	1700	55	16.6	0.0003
M3A	2150	520	13.5	0.002

change in the circulator characteristics was small, a slight increase in circulation frequency occurred.

A. Simple Rod Y-Junction Circulator

The numerical test for the accuracy of the results is the same as has been discussed in a previous paper [9]. It is found that four cylindrical modes in regions 1 and 2, four TE waveguide modes, and two TM waveguide modes give reasonably accurate results.

1) Circulator Characteristics: Fig. 5 shows the circulator characteristics obtained by the numerical method using the point matching technique. Also shown in the same figure are the experimental results obtained using ferrite material Y13A with the following dimensions: 0.15-in radius and 0.9-in height. It is clear from this figure that the general shapes of both characteristic curves obtained by both methods are nearly the same. The numerical and experimental results of the reflection coefficient characteristic are very close and the difference between them is of the order of 1 dB or less. The maximum difference between the numerical and experimental results in both the isolation and insertion loss curves is of the order of 1.5 and 2 dB and takes place at 10 and 10.5 GHz, respectively; still the general shapes of the curves are the same which confirms the correctness of the analysis and the correct choice of the number of modes in each region. It should be noticed that there is no circulation in the entire X band because the ferrite rod radius is too large. The frequencies 9.25 and 12.0 GHz have minimum reflection but do not represent points of circulation because the output power is divided between the other two ports. There is approximately a complete reflection at 11.0 GHz.

Fig. 6 shows the computed circulator characteristics when using ferrite with a radius of 0.1 in. In this case, the circulation frequency occurs at 10.6 GHz, while the minimum insertion loss and minimum reflection take place at 10.8 GHz. The value of isolation at the circulation frequency is about 12 dB, while the reflection and insertion loss are 12.5 and 0.495 dB, respectively. At the upper end of the frequency band another point of very poor circulation appears in the same direction, while at 12.0 GHz a large part of the incident power is reflected back from the input port (reflection coefficient equals 3.176 dB, i.e., 0.4813 in ratio).

Davis and Longely [3] stated that "a single broadband mode of circulation can be found using ferrite posts, provided that the diameter is less than 0.2 inch." From the numerical results, it is observed that a simple mode of circulation may occur when the ferrite diameter is greater than 0.16 in and less than or equal to 0.24 in. When increasing the ferrite diameter above this value complicated characteristics are obtained and circulation may not take place.

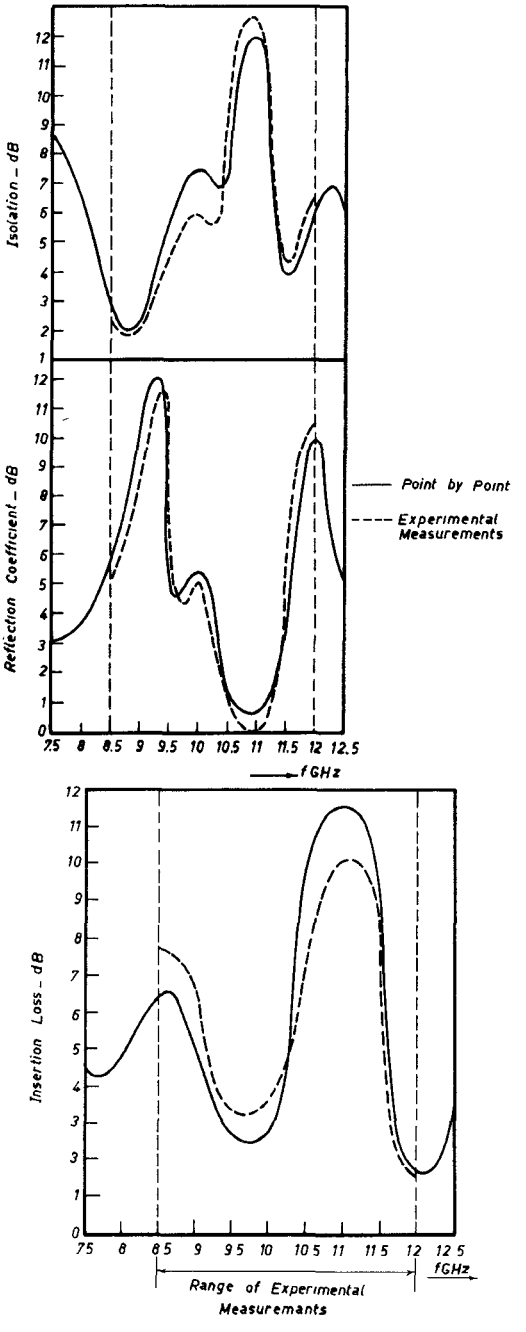

Fig. 5. Circulator characteristics for the Y-junction circulator, $R = 0.15$ in.

The variation of the circulation frequency (the frequency of maximum isolation) with the ferrite radius, for a constant dc magnetic field (200 Oe) using both ferrite materials Y13A and M3A, is shown in Fig. 7. It is clear from this figure that when the ferrite radius is increased, the circulation frequency decreases, approximately linearly. This statement holds for both ferrite materials. This behavior is the same as that of the H-plane circulator [9].

This result can be explained physically as follows: The magnetic field for the TE_{10} mode in the XY plane can be considered approximately circularly polarized with a different sense of polarization in each side of the X axis. The effect of the ferrite rod is to increase the wavelength of the wave in one side and to decrease the wavelength in the other side of

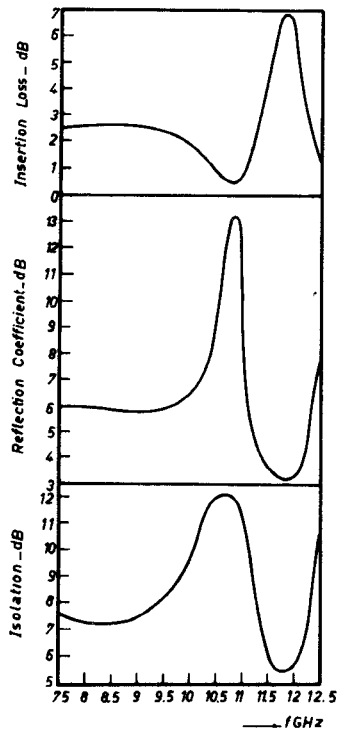

Fig. 6. Circulator characteristics for the Y-junction circulator, $R = 0.10$ in.

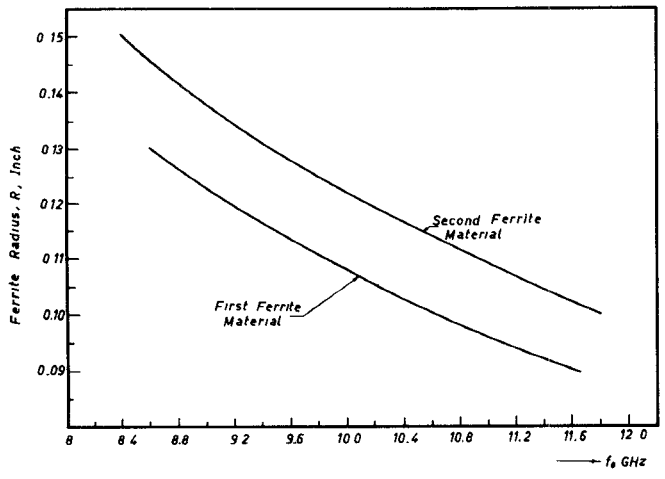

Fig. 7. Ferrite radius R_f versus frequency of maximum isolation f_0.

the X axis. Therefore, the wavefront after passing through the ferrite rod will not be perpendicular to the X axis, but will be tilted through an angle. Circulation will take place when this angle is $2\pi/3$. When the ferrite radius increases the same angle of rotation for the phase front is obtained at a lower frequency.

On the basis of the results shown in Fig. 7 it is possible to design X-band E-plane circulators theoretically.

2) *Power Density Distributions in Regions 1 and 2:* One of the most important advantages of the point matching technique is that it enables one to know the fields and consequently the power density distributions inside the junction. Once the set of inhomogeneous equations is solved by the digital computer, the complex amplitudes in the ferrite rod $A_{m,n1}$ and $A_{m,n2}$ are known and, consequently, $F_{m,n1}$, $F_{m,n2}$, $H_{m,n1}$, and $H_{m,n2}$ are obtained. The fields and consequently the power density distributions at any point (r,θ,z) can be obtained from the field expressions (6)–(9) and (10)–(13).

Fig. 8 shows the power density distribution in the ferrite rod, for the case of $R = 0.1$ in at a circulation frequency of 10.6 GHz. The radial power flow along a cylindrical shell opposite any waveguide is given by the area under the curve extending along that arc multiplied by the arc radius. From the figure it is seen that P_r is zero near the axis of the isolated port, while the net area along the isolated port is approximately zero since the positive part is approximately equal to the negative part. The area under the curve along the arc opposite the input port is approximately equal to the area under the curve along the arc opposite the output port, but with a different sign as has been mentioned in [9]. The reason for this is that the power in the input port is incident to the junction, while the power in the output port is leaving the junction.

From Fig. 8, it can be seen that as the ferrite radius increases, P_r is reduced in order to keep the area under the curve multiplied by the corresponding radius constant.

It should be noted that when the power density distribution is plotted for the frequency of minimum insertion loss (10.8 GHz), the area under the curve opposite the input and output ports increases. This happens because of the fact that when the insertion loss is minimum, almost all the input power comes out from the output port with minimum reflection from the input port.

B. Simple Rod T-*Junction Circulator*

Numerical results for both types of T-junctions are presented in this section. In the first type (Fig. 3) the imaginary boundary (cylindrical boundary) is not complete since it is cut by the perfect conductor 1–4. This reduces the accuracy of the results greatly [11] as compared with the excellent accuracy obtained in the case of the Y-junction circulator. Another factor which causes a reduction in the accuracy of the results for both types of T junction, when using the point matching technique in solving the problem, is the lack of axial symmetry in the T-junction circulator compared with the Y-junction circulator.

The circulator characteristics for the first type of T junction have been obtained numerically using the Y13A ferrite material and different ferrite rod radii. The case of $R = 0.11$ in is shown in Fig. 9. A very sharp circulation is observed at 11.95 GHz, and a large reflection takes place at the lower and upper ends of the frequency band (7.5 and 12.5 GHz) and also at 9.0 GHz. The circulator characteristics have also been obtained for the second type of T junction using the ferrite materials Y13A and M3A with different ferrite rod radii. The case of $R = 0.11$ in using the first ferrite material is shown in Fig. 10. It is observed that in the case of T junctions circulation takes place at a higher frequency than in the case of Y junctions. Also, it is found that the circulator characteristics in both cases are completely different. However, the general shape of the characteristic curves of both types of T junction are alike, except for a shift

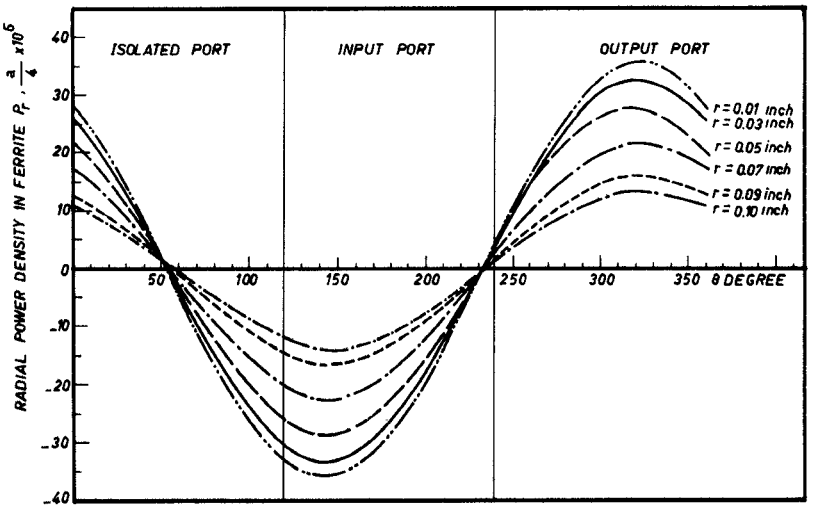

Fig. 8. Radial power density distribution in a ferrite rod at 10.6 GHz.

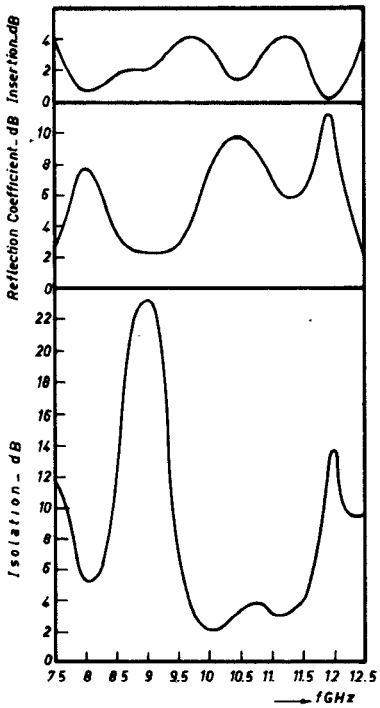

Fig. 9. Circulator characteristics for the T-junction circulator (first type), $R = 0.11$ in.

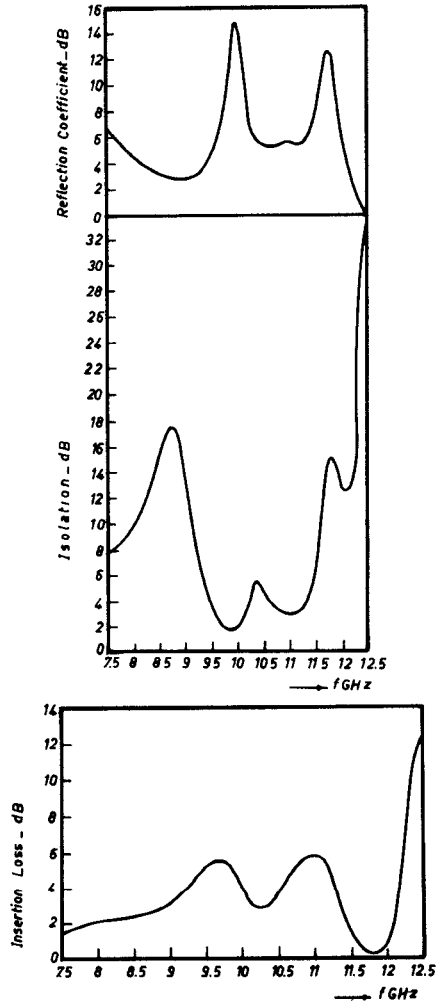

Fig. 10. Circulator characteristics for the T-junction circulator (second type), $R = 0.11$ in.

toward the lower frequency in the case of the second type of T junction.

Fig. 11 shows the variation of the ferrite radius with the frequency of maximum isolation, for both types of T junction when the internal dc magnetic field is 200 Oe. The results shown in this figure are a useful guide for the theoretical design of X-band T-junction circulators.

IV. Conclusions

The point matching technique has been used successfully to obtain the circulator characteristics for three types of E-plane junctions. It is found that the circulation frequency for the T junction in which the perfect conducting surface is a plane (first type) is higher than that for the T junction in which the perfect conducting surface is cylindrical (second type). The circulation frequency for the second type of T junction is higher than that for the Y junction when using the same ferrite material and the same ferrite rod radius. For the

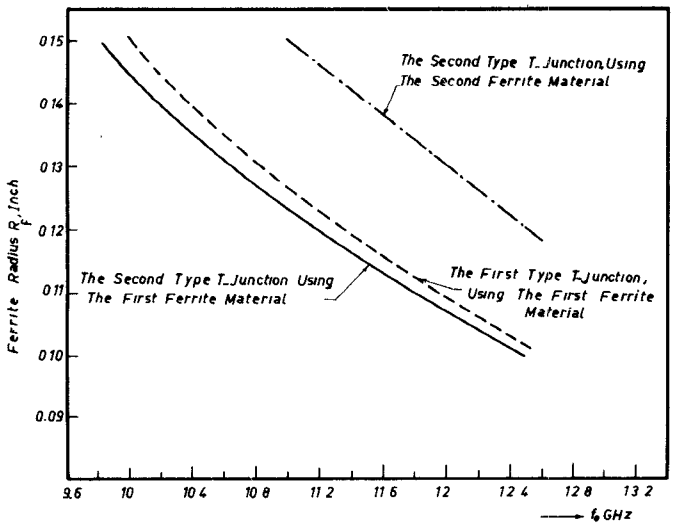

Fig. 11. Ferrite radius R_f versus frequency of maximum isolation f_0 for both types of T junction.

three different types of junctions, the circulation frequency decreases with increases in the ferrite radius.

No single mode of circulation is found for the Y-junction circulator when the ferrite diameter increases above 0.24 in, but rather complicated characteristics are found. When the ferrite diameter is reduced below 0.16 in, no circulation occurs and the characteristics become flat.

The power density distributions, in the ferrite rod and the air ring surrounding it, have been obtained and plotted. These curves indicate the distribution of the incident power among the different ports.

Experimental measurements have been carried out for one sample of ferrite and show good agreement with the corresponding numerical results. The bandwidth obtained is very narrow which is expected, since no provision has been made for bandwidth enlargement. It is expected that dielectric loading can be used effectively to increase the bandwidth.

REFERENCES

[1] S. Yoshida, "*E*-type *X*circulator," *Proc. IRE* (Lett.), vol. 47, p. 2017, Nov. 1959.

[2] ——, "An *E*-type T circulator," *Proc. IRE* (Lett.), vol. 47, p 2018, Nov. 1959.

[3] L. E. Davis and S. R. Longley, "*E*-plane 3-port *X*-band waveguide circulators," *IEEE Trans. Microwave Theory Tech.* (Correspond.), vol. MTT-11, pp. 443–445, Sept. 1963.

[4] G. Buchta, "Miniaturized broadband *E*-tee circulator at *X*-band," *Proc. IEEE* (Lett.), vol. 54, pp. 1607–1608, Nov. 1966.

[5] J. Helszajn and M. McDermott, "Mode chart for *E*-plane circulators," *IEEE Trans. Microwave Theory Tech.* (Correspond.), vol. MTT-20, pp. 187–188, Feb. 1972.

[6] W. H. Wright, Jr., and J. W. McGrowan, "High power Y-junction *E*-plane circulator," *IEEE Trans. Microwave Theory Tech.* (Correspond.), vol. MTT-16, pp. 557–559, Aug. 1968.

[7] E. E. DeCamp, Jr., and R. M. True, "1 MW four-port *E*-plane junction circulator," *IEEE Trans. Microwave Theory Tech.* (Correspond.), vol. MTT-19, pp. 100–103, Jan. 1971.

[8] A. P. Darwent, "Symmetry in a high power circulator for 35 GHz," *IEEE Trans. Microwave Theory Tech.* (Correspond.), vol. MTT-15, p. 120, Feb. 1967.

[9] M. E. El-Shandwily, A. A. Kamal, and E. A. F. Abdallah, "General field theory treatment of *H*-plane waveguide junction circulators," *IEEE Trans. Microwave Theory Tech.*, vol. MTT-21, pp. 392–403, June 1973.

[10] R. F. Soohoo, *Theory and Application of Ferrites.* Englewood Cliffs, NJ: Prentice-Hall, Inc., 1960.

[11] L. Lewin, "On the inadequacy of discrete mode-matching techniques in some waveguide discontinuity problems," *IEEE Trans. Microwave Theory Tech.*, vol. MTT-18, pp. 364–372, July 1970.

[12] S. W. Lee, W. R. Jones, and J. J. Campbell, "Convergence of numerical solutions of iris type discontinuity," *IEEE Trans. Microwave Theory Tech.*, vol. MTT-19, pp. 528–536, June 1971.

[13] Alvin Wexler, "Solution of waveguide discontinuities by modal analysis," *IEEE Trans. Microwave Theory Tech.*, vol. MTT-15, pp 508–517, Sept. 1966.

[14] J. B. Davies, "A least squares boundary residual method for the numerical solution of scattering problems," *IEEE Trans. Microwave Theory Tech.*, vol. MTT-21, pp. 99–104, Feb. 1973.